Radiomics-based distinction of small (≤2cm) HCC and precancerous lesion based on precontrast MRI

XiaoNing Gao (748117050@qq.com)
Tangshan Central Hospital
JiaWen Luo
the Second Affiliated Hospital of Dalian Medical University
Kun Guo
the Second Affiliated Hospital of Dalian Medical University
Yue Xiang
the Second Affiliated Hospital of Dalian Medical University
Hao Liu
Yizhun Medical AI Co., Ltd
Jia Ding
Yizhun Medical AI Co., Ltd

Research Article

Keywords: Radiomics, S-HCC, MRI

Posted Date: April 26th, 2022

DOI: https://doi.org/10.21203/rs.3.rs-1202840/v1

Abstract

Background: The pre-HCC describe the precancerous condition of HCC, which include regenerative nodule (RN), low-grade dysplastic nodule (LGDN) and high-grade dysplastic nodule (HGDN) [1].

Purpose: To assess the feasibility of radiomics based on precontrast MRI for the distinguish of small hepatocellular carcinoma (S-HCC) (≤2cm) and pre-hepatocellular carcinoma (pre-HCC).

Method: We retrospectively analyzed 146 nodules with pathological confirmed from 78 patients. Each nodule was segment on precontrast MRI sequence (T1WI and fat-suppression T2WI (FS-T2WI)), retrospectively. 1223 radiomics features were extracted and the optimal features from T1WI, FS-T2WI and T1WI+FS-T2WI were selected by the least absolute shrinkage and selection operator (LASSO). We used the logistic regression classifier to establish the radiomics model.

Result: We applied logistic regression classifier to identify S-HCC and pre-HCC on the basis of valuable radiomics features extracted from T1WI, FS-T2WI, T1WI+FS-T2WI, respectively. The AUC, sensitivity and specificity of the training group and test group based on T1WI were 0.879 (95% CI 0.797 -0.962), 78.9% and 83.1% and 0.796 (95% CI 0.619-0.973), 66.7% and 83.3%, respectively. The AUC, sensitivity and specificity of the training group and test group based on FS-T2WI were 0.911 (95% CI 0.839-0.983), 94.7% , 83.1% and 0.907 (95% CI 0.779-1), 83.3%, 88.9%, respectively. The AUC, sensitivity and specificity of the training group and test group based on T1WI+FS-T2WI were 0.918 (95% CI 0.844-0.991), 84.2% , 87.3% and 0.870 (95% CI 0.728-1), 84.2%, 87.3%, respectively.

Conclusion: This study suggested that radiomics model may serve as an adjunct and noninvasive tool to classify S-HCC and pre-HCC based on precontrast MRI.

Background

Hepatocellular carcinoma (HCC) is the fifth most common tumor and the second most fatal cancer in the world [2]. The high risk of HCC include hepatitis viruses, alcohol, non-alcohol fatty liver disease and inherited metabolic diseases [3]. Most HCC develops through a multistep processes, called hepatocarcinogensis, in which RN, LGDN and HGDN (referred as pre-HCC) evolves into early-HCC (E-HCC) and progressed-HCC (P-HCC) gradually [4, 5]. The prognosis of HCC depends largely on the stage at which the tumor is detected [6]. In patients who present with symptoms, median survival is less than 1 year and the 5-year survival is less than 10% [7]. By contrast, Patients may benefit from life-prolonging, potentially curative treatments in the early development of HCC [8]. Some clinical studies had shown that clinical surgical intervention for S-HCC (≤ 2cm) can reduce the recurrence rate and improve the cure rate of patients [9–11]. Therefore, the early detection of S-HCC and differentiation of S-HCC from pre-HCC are of great significance for patients. All current guidelines recommend surveillance for patients at high risk. In general, CT and MRI with contrast agent are commonly used. However, the detection and characterization of S-HCC in cirrhotic patients is still challenging cause it's difficult to distinguish them from other lesion that could develop in cirrhotic liver, especially HGDNs, due to the overlap of imaging

features [12]. At present, Gd-EOB-DTPA MRI and DWI are also commonly used to improve the detection rate and diagnostic accuracy of S-HCC. Renzulli et al. demonstrated that a new diagnostic algorithm combined Gd-EOB-DTPA MRI with DWI could evaluate all the lesions in cirrhotic liver, including E-HCC and HGDN [13]. However, diagnosis may be problematic in patients who cannot undergo enhancement inspection cause of contraindications. Moreover, repeated enhancement examinations will increase the burden of patients. We urgently need a more convenient and noninvasive method.

Radiomics, as a quantitative noninvasive analysis method, has shown great application value in diagnosis, evaluation of curative effect and prognosis. Gato et al. suggested that radiomic can classify focal liver lesions based on non-enhanced T2-weighted images [14]. Wu et al. showed that radiomics can be used to distinguish between HCC and hepatic haemangioma on precontrast images [15]. Li et al. reported texture features of SPAIR T2WI-MRI can classify the three types of single liver lesions (hepatic hemangioma, hepatic metastasis and HCC) [16]. Our study aims to assess the feasibility of radiomics based on precontrast MRI for differentiation of S-HCC and pre-HCC.

Material And Methods

Patient

This is a retrospective study. Between September 2017 and February 2020, 82 patients were included in this study and performed precontrast MRI. The inclusion criteria: cirrhotic patient; no interventional therapy was performed before surgery; MRI examination was performed within two weeks before surgery; performed by the same scanning machine and parameters; pathological confirmation of RN, DN and HCC verified by resection or liver transplantation. The exclusion criteria: the lesion was not clearly shown on precontrast MRI; nodule was larger than 2cm; the gross specimen did not correspond to the location or size of the nodule shown in the imaging. Patients were randomly allocated to training and test groups in a ratio of 8:2. Our Institutional Ethic Review Board has approved this study, following the Declaration of Helsinki.

MRI acquisition

All enrolled patients were examined with 3.0T MRI (Verio; Siemens, Erlangen, Germany), with 8-channel body phased array coil and TSE sequence acquisition collection under respiratory trigger. Abdominal pressure band was applied to the lower abdomen of the patient to reduce artifacts caused by abdominal respiratory movements. The MR scan sequence included: fast low angle shot (FLASH) T1WI sequence imaging, and turbo spin-echo (TSE) T2WI navigation trigger axial imaging. We only list the parameters of TIWI and axial fat-suppression T2WI shown in Table 1.

Table 1
MRI conventional sequence parameter

	TR ms	TE(ms)	Matrix	thickness (mm)	slice gap (mm)	NEX
Axial T1WI	4.20	1.26	320·240	3	0.6	1
Axial T2WI-FS	2000	84	320·320	5	1.5	1

Pathological examination

Refer to the MRI, the resected or transplantation liver specimens were cut at an interval of nearly 1cm. Specimens were sectioned, dehydrated and paraffin-embedded, stained with hematoxylin-eosin (HE), and then subjected to histological and immunohistochemical examination. The pathological diagnosis of nodule was evaluated according to the International Consensus Group for Hepatocellular Neoplasia criteria. Two pathologists with more than 10 years of experience in HCC pathology reviewed all the specimen slices independently, without knowing the patients' clinical data.

Establishment of radiomics model

1. Segmentation

The volumes of interests (VOIs) were manually delineated around each nodule's outline for 3D volume as indicated in TIWI and FS-T2WI by two independent radiologists with more than 5 years of experience in abdominal diagnosis using the Medical Standard - Darwin Intelligent Scientific Research Platform (Beijing, Yizhun Medical AI Co., Ltd). Segmentation was checked by a radiologist with over 10 years of experience in abdominal diagnosis. They were all blinded to clinical history and pathology results, but aware of the study's purpose and method of the study, as well as the location of the nodule.

2. Extraction and selection

The first step was the normalization of image quantitative data. We normalized the pixels to 1:1:1, and linearly normalized the grayscale values from 0 to 4096. Then, the radiomics features were extracted from the image by mathematical algorithm software, including first-order features, 2D and 3D shape features, second-order features (namely texture features, including gray-level co-occurrence matrix (GLCM) features, gray-level run-length matrix (GLRLM) features, gray-level size zone matrix (GLSZM) features, gray-level dependence matrix (GLDM) features, and neighbourhood gray-tone difference matrix (NGTDM) features)) and high-order features [16]. A total of 1223 radiomics features were extracted from each sequence (Supplementary Information, Table 1). To avoid overfitting, the LASSO algorithms was applied for dimensionality reduction. Finally, the optimal features were selected from each single sequence and combine sequence (T1WI+FS-T2WI).

3. Establishment of radiomics model

Logistic Regression classifier (LR) was applied to establish each radiomics model using the optimal radiomics features [15]. Radiomics models were evaluated using the area under the receiver operating characteristic curve (AUC), sensitivity, specificity.

Statistic analysis

Categorical variable were compared using the X^2 test. Continuous variable were compared using the Student t test. The p value less than 0.05 was considered to indicate statistical significance. Statistical analysis were carried out using SPSS version 23 (IBM software) and the Medcale statistical software (http://www.medcalc.org). Radiomics feature extraction, dimension reduction and model establishment were accomplished by the Medical Standard - Darwin Intelligent Scientific Research Platform (Beijing, Yizhun Medical AI Co., Ltd).

Result

1. Characteristics of patients and nodules

A total of 78 patients with 114 nodules were included in the study except 4 patients who had severe ascites. 70 patients had chronic hepatitis B cirrhosis, 3 patients had chronic hepatitis C cirrhosis, 3 patients had autoimmune cirrhosis, and 2 patients had alcoholic cirrhosis. There were 89 S-HCCs and 25 pre-HCCs, including 3 DNs and 22 RNs. The training group included 90 nodules (pts.: 71 S-HCC/19 pre-HCC), and the test group included 24 nodules (pts.: 18 S-HCC/6 pre-HCC). The patients' and nodules' characteristics were shown in Table 2.

Table 2
Patients' and nodules' characteristics

Patients' date		value	
gender	male	62	
	female	16	
	total	78	
age	average	58.6±1.45	
Pathology			P values
S-HCC (n=90)	Training group	71	0.682
	Test group	19	
			P values
pre-HCC (n=90)	Training group	18	0.682
	Test group	6	

2. Radiomics models

The flow chart for the establishment of radiomics model is shown in Fig. 1.

The optimal radiomics features (n=8) and radiomics scores obtained based on T1WI are shown in Formula 1. The AUC, sensitivity and specificity of the training group were 0.879 (95% CI 0.797-0.962), 78.9% and 83.1%, respectively. The AUC, sensitivity and specificity of the test group were 0.796 (95% CI 0.619-0.973), 66.7% and 83.3%, respectively. The ROCs of the models are shown in Fig. 2.

RadScore = +0.737*T1WI_wavelet-LHL_glcm_InverseVariance-

0.552*T1WI_wavelet-HLL_firstorder_Median-

0.499*T1WI_wavelet-HLL_firstorder_Mean-

0.470*T1WI_squareroot_glcm_ClusterShade+

0.278*T1WI_wavelet-LHL_firstorder_InterquartileRange+

0.197*T1WI_wavelet-LHL_firstorder_RobustMeanAbsolutrDeviation+

0.061*T1WI_squareroot_glszm_ZonePercentage-

0.004*T1WI_wavelet-HLL_firstorder_10Percentile-1.670

Formula (1)

The optimal radiomics features (n=8) and the radiomics score obtained based on FS-T2WI are shown in Formula 2. The AUC, sensitivity and specificity of the training group were 0.911 (95% CI 0.839-0.983), 94.7% and 83.31%, respectively. The AUC, sensitivity and specificity of the test group were 0.907 (95% CI 0.779-1), 83.3%, and 88.9%, respectively. The ROCs of the models are shown in Fig. 3.

RadScore = +0.556*T2WI_wavelet-HLL_firstorder_Mean+

0.527*T2WI_logarithm_glszm_ZonePercentage-

0.498*T2WI_square_glszm_SizeZoneNonUniformityNormalized+

0.384*T2WI_square_gldm_DependenceNonUniformityNormalized+

0.351*T2WI_wavelet_LHL_firstorder_Mean+

0.267*T2WI_wavelet_LHL_glszm_SizeZoneNonUniformityNormalized-

0.125*T2WI_logarithm_firstorder_10Percentile+

0.041*T2WI_wavelet-HLL_ngtdm_Contrast-1.973

Formula (2)

The optimal radiomics features (n=9) and the radiomics score obtained based on T1WI+FS-T2WI are shown in Formula 3. The AUC, sensitivity and specificity of the training group were 0.918 (95% CI 0.844-0.991), 84.2% and 87.3%, respectively. The AUC, sensitivity and specificity of the test group were 0.870 (95% CI 0.728-1), 84.2%, and 87.3%, respectively. The ROCs of the models are shown in Fig. 4.

RadScore = +0.788*T2WI_square_gldm_DependenceNonUniformityNormalized+

0.692*T1WI_wavelet_LHL_glcm_InverseVariance+

0.597*T2WI_square_glszm_SizeZoneNonUniformityNormalized-

0.525*T1WI_wavelet-HLL_firstorder_Median-

0.523*T1WI_wavelet_HLL_firstorder_Mean+

0.181*T1WI_wavelet_LHL_firstorder_InterquartileRange-

0.083*T1WI_wavelet_HLL_firstorder_10Percentile-

0.079*T1WI_wavelet-LHL_firstorder_10Percentile-

0.012*T1WI_squareroot_glszm_ZonePercentage-1.849

Formula (3)

The ADC, sensitivity and specificity of the three radiomics models was shown in Table 3.

Table 3
diagnostic performance of radiomics models

Radiomics model	train			test		
	sensitivity	specificity	AUC	sensitivity	specificity	AUC
T1	0.789	0.831	0.879	1	0.677	0.796
T2	0.947	0.831	0.911	1	0.778	0.917
T1+FS-T2	0.842	0.873	0.918	0.842	0.873	0.870

Discussion

This study demonstrates that radiomics model can be trained to distinguish S-HCC and pre-HCC based on precontrast MRI. We also found the FS-T2WI shows better performance on single sequence.

The radiomics features categorized into first-order features, shape features, second-order texture features and higher-order features. First-order features describe the intensity characteristics of tumors, and are general and basic indicators to describe the distribution of voxel intensity within the image region. Shape features described the three-dimensional dimensions, size, and shape of the lesion area, and were used to describe the characteristics of tumors with spherical or aspirated shapes. Second-order features, namely texture features, could quantify the heterogeneity within the tumor and represent the three-dimensional spatial characteristics of the lesion. Higher-order statistics features were robust features transformed from the first- and second-order features by filers. Five types of filters were applied: exponential, square, square root, logarithm and wavelet (which was applied as either a high- (H) or a low-pass(L)filter in each of the three dimensions: wavelet-LHL, wavelet-LHH, wavelet-HLL, wavelet-LLH, wavelet-HLH, wavelet-HHH, wavelet-HHL, wavelet-LLL) [15]. In present study, we obtained meaningful radiomincs feature sets from precontrast MRI, in which higher-order statistics features provided significant role. We also found the shape features were the most in efficient. It might because the lesion is too small and the image layer is too thick, the shape of the lesion could not be used to distinguish S-HCC from pre-HCC.

We found that the radiomics model based on FS-T2WI shows the better performance on single sequence. We would like to elaborate them combining the definitions of the radiomics features. The optimal radiomics features extracted from FS-T2WI mainly including the higher-order features which transformed from some first-order and second-order features. Next, we would introduce the meaning of the related radiomics features. Firstorder-Mean means the average gray level intensity within the ROI. Firstorder-10th percentile means the 10th percentile of the set of voxels included in the ROI. They were first-order features related to the intensity of the nodule [17]. GLSZM_size zone non-uniformity measures the variability of size zone volumes throughout the image, with a lower value indicating more homogeneity among zone

size volumes in the image. And GLSZM_zone percentage measures the coarseness of the texture by taking the ratio of number of zones and number of voxels in the ROI. GLDM_dependence non-uniformity normalized measures the similarity of dependence throughout the image, with a lower value indicating more homogeneity among dependengcies in the image. NGTDM_contrast is a measure of the spatial intensity change, and it also dependent on the overall gray level dynamic range, for example, an image with a large range of gray level, with large changes between voxels and their neighbourhood [17]. These second-order features describe heterogeneity of lesions.

The effective features may be associated with different pathological characteristics during hepatocarcinogenesis. First, growing evidences suggest that chronic inflammation causes repeated cycles of cell injury, death and regeneration, which promoting aberrant cell signaling, epigenetic changes, mutational events, and accumulation of genetic damage [18–21]. During this phase, phenotypic and alteration occurred. Second, angiogenesis progresses is one of the key structural alteration during hepatocarcinogenesis, which is characterized by the presence of unpaired arteries and sinusoidal capillarization. Meanwhile, the portal tracts progressively diminish [19, 20, 22, 23]. Third, in cirrhotic livers, fat and iron content may change in hepatocytes. Because in the transition phase from portal to arterial supply, there is a period in which the development of unpaired arteries is not sufficient to compensate for the reduced portal venous and nontumoral arterial flow [24]. The change of fat and iron content is though to be associated with ischemic environment. In a word, these pathological characteristic may affect the signal of the lesion and cause heterogeneity within the lesion.

And why FS-T2WI features showed better performance? We speculate that there may be several reasons. First of all, as is well-known, most tumors have higher intracellular and/or extracellular water content than normal tissues. This may be related to the heterogeneity of tumor cells. Heterogeneity can be manifested in abnormal cell size, cell pleomorphism, nucleus-cytoplasm ratio, etc. During hepatocarcinogenesis, with the mutation of the gene, affected cells composed of pre-HCC and S-HCC acquire progressively atypical phenotypic features [25], and the corresponding water content of the cells is also different, which maybe reflected in T2 signal intensity. In addition, Shinmura et al. found that there was a significant association between the intranodular portal venous and arterial blood supplies and the T2-weighted MR imaging signal intensity in various types of hepatocellular nodules associated with liver cirrhosis [21]. Namely, the signal intensity on T2-weighted MR images increased as the intranodular portal venous blood supply decreased and arterial supply increased [21]. This conclusions may also be applicable to distinguish S-HCC and pre-HCC. Moreover, in terms of the step of delineating lesions in the radiomics study, a more complete radiomics feature of lesions can be obtained from T2WI because the edges of lesions can be more clearly and accurately identified by naked eye. This random errors may also cause differences between the performance of radiomics models based on T1WI or T2WI [26].

This study confirmed that radiomics can be used to distinguish S-HCC from pre-HCC based on precontrast MRI. And the radiomics model based on FS-T2WI showed the better performance on single sequence. Mokrane et al validated Delta V-A_DWT_LL_Variance-2D, a single radiomics feature of CT, which quantifying changes between arterial and portal venous phases can diagnose HCC in cirrhotic

patients with indeterminate liver nodules [27]. In our study, radiomic models were based on precontrast MRI, which were more convenience and ignoring the contraindication of enhanced scanning. Cause of the repeatability and non-fatigue characteristics of the radiomics, it might has potential clinical application value. In this study, we delineated around each lesion outline for 3D volume area to obtain whole radiomics features as far as possible. To make precise classification, we certified all lesions by postoperative pathology. Thus, it was a reliable and noninvasive method for differential diagnosis between S-HCC and pre-HCC.

There are several limitations. Firstly, the sample size was small. A large number date from multi-center should validate and improve the generalisability of our finding. Secondly, other MRI sequences, such as in-, out-phase and DWI, should be enrolled in further studies. Thirdly, clinical characteristic might be helpful in distinguishing S-HCCs from pre-HCCs and should be further studied.

Conclusion

This study suggested that radiomics model may serve as an adjunct and noninvasive tool to classify S-HCC and pre-HCC based on precontrast MRI.

Abbreviations

AUC: Area under receiver operating characteristic curve; GLCM: Gray-level co-occurrence matrix; GLDM: Gray-level dependence matrix; HCC: Hepatocellular carcinoma; HGDN: High grade dysplastic nodule; LGDN: Low grade dysplastic nodule; LR: Logistic regression; MRI: Magnetic resonance imaging; NGTDM: Neighbourhood gray-tone difference matrix; Rad score: Radiomics score; RN: Regenerative nodule; ROC: Receiver operating characteristic curve; S-HCC: small-Hepatocellular carcinoma; TSE: Turbo spin-echo; VOI: volume of interest

Declarations

Acknowledgements

The authors wish to thank Hao Liu, Ph.D. and Jia Ding, Ph.D. for their technical support in the instructions of the radiomics analysis.

Funding

There is no funding.

Availability of data and materials

The datasets generated and/or analysed during the current study are not publicly available due to patient privacy protection, but are available from the corresponding author on reasonable request.

Authors' contribution

XNG and JWL conceived the research, executed the experiments, and wrote the manuscript. XNG, KG and YX did some work in performing the experiments. HL and JD analyzed the result. All authors read and approved the final manuscript for publication.

Ethics approval and consent to participate

This study was approved by the institutional review board at the corresponding author's institution(The Second Affiliated Hospital of Dalian Medical University), and follow the principles of the 1964 Declaration of Helsinki and subsequent amendments. Informed consent was obtained from all patients. The consent obtained from study participants was verbal because this retrospective study has been approved by the ethics committee at the corresponding author's institution.

Consent for publication

Consent for publication of individual persons' images was obtained from these persons.

Competing interests

The authors declare that they have no competing interests.

References

1. Y Yang, Liu C, Qi L, et al. Diagnosis of Pre-HCC Disease by Hepatobiliary-Specific Contrast-Enhanced Magnetic Resonance Imaging: A Review[J]. Digestive Diseases and Sciences, 2019, 65(9).
2. Heimbach JK, Kulik LM, Finn RS, Sirlin CB, Abecassis MM, Roberts LR, et al. AASLD guidelines for the treatment of hepatocellular carcinoma. Hepatology 2018;67:358–380.
3. AMD Bisceglie. Hepatitis B and hepatocellular carcinoma[J]. Hepatology, 2009.
4. Coleman WB. Mechanisms of human hepatocarcinogenesis. Curr Mol Med. 2003;3:573–88.
5. Efremidis SC, Hytiroglou P. The multistep process of hepatocarcinogenesis in cirrhosis with imaging correlation. Eur Radiol. 2002;12:753–64.
6. McGlynn KA, London WT. Epidemiology and natural history of hepatocellular carcinoma. Best Pract Res Clin Gastroenterol 2005;19 (1): 3–23.
7. Elserag HB, DM, Ph M. Hepatocellular carcinoma.[J]. New England Journal of Medicine, 2011, 365(12):1118–27.
8. Choi JY, Lee JM, Sirlin CB. CT and MR Imaging Diagnosis and Staging of Hepatocellular Carcinoma: Part I. Development, Growth, and Spread: Key Pathologic and Imaging Aspects[J]. Radiology, 2014, 272(3):635–654.
9. Takayama T, Makuuchi M, Hirohashi S, et al. Early hepatocellular carcinoma as an entity with a high rate of surgical cure. Hepatology 1998; 28:1241–46.

10. Midorikawa Y, Yamamoto S, Tsuji S, et al. Allelic imbalances and homozygous deletion on 8p23.2 for stepwise progression of hepatocarcinogenesis. Hepatology 2009;49:513–22.
11. Yamamoto M, Takasaki K, Otsubo T, et al. Favorable surgical outcomes in patients with early hepatocellular carcinoma. Ann Surg 2004; 239:395–9.
12. MD Martino, Anzidei M, Zaccagna F, et al. Qualitative analysis of small (≤2cm) regenerative nodules, dysplastic nodules and well-differentiated HCCs with gadoxetic acid MRI[J]. Bmc Medical Imaging, 2016, 16(1):62.
13. Renzulli M, Biselli M, Brocchi S, et al. New hallmark of hepatocellular carcinoma, early hepatocellular carcinoma and high-grade dysplastic nodules on Gd-EOB-DTPA MRI in patients with cirrhosis: A new diagnostic algorithm. Gut, 2018, 67(9): 1674–1682.
14. Gatos I, Tsantis S, Karamesini M, et al. Focal liver lesions segmentation and classification in nonenhanced T2-weighted MRI[J]. Medical Physics, 2017, 44.
15. Wu J, Liu A, Cui J, et al. Radiomics-based classification of hepatocellular carcinoma and hepatic haemangioma on precontrast magnetic resonance images[J]. BMC Medical Imaging, 2019, 19(1).
16. Li Z, Yu M, Wei H, et al. Texture-based classification of different single liver lesion based on SPAIR T2W MRI images[J]. BMC Medical Imaging, 2017, 17(1):42.
17. Zwanenburg A, Leger S, M Vallières, et al. Image biomarker standardisation initiative[J]. Radiotherapy & Oncology, 2016.
18. Trevisani F, Cantarini M C, Wands J R, et al. Recent advances in the natural history of hepatocellular carcinoma.[J]. Carcinogenesis, 2008(7):1299.
19. Ueda K, Matsui O, Kawamori Y, et al. Hypervascular hepatocellular carcinoma: evaluation of hemodynamics with dynamic CT during hepatic arteriography.[J]. Radiology, 1998, 206(1):161–6.
20. Kitao A, Zen Y, Matsui O, et al. Hepatocarcinogenesis: multistep changes of drainage vessels at CT during arterial portography and hepatic arteriography--radiologic-pathologic correlation.[J]. Radiology, 2009, 252(2):605–614.
21. Shinmura R, Matsui O, Kobayashi S, et al. Cirrhotic nodules: association between MR imaging signal intensity and intranodular blood supply.[J]. Radiology, 2005, 237(2):512.
22. Palmer WC, Patel T. Are common factors involved in the pathogenesis of primary liver cancers? A meta-analysis of risk factors for intrahepatic cholangiocarcinoma[J]. JOURNAL OF HEPATOLOGY, 2012.
23. Coleman, WB. Mechanisms of human hepatocarcinogenesis. Curr Mol Med 3: 573-588[J]. Current Molecular Medicine, 2003, 3(6):573-588.
24. Kutami R, Nakashima Y, Nakashima O, et al. Pathomorphologic study on the mechanism of fatty change in small hepatocellular carcinoma of humans[J]. 2000, 33(2):282–289.
25. Xin WW, Hussain SP, Huo TI, et al. Molecular pathogenesis of human hepatocellular carcinoma[J]. Toxicology, 2003, 181–182(1-3):43–47.

26. Wu J, Liu A, Cui J, et al. Radiomics-based classification of hepatocellular carcinoma and hepatic haemangioma on precontrast magnetic resonance images[J]. BMC Medical Imaging, 2019, 19(1).
27. Radiomics machine-learning signature for diagnosis of hepatocellular carcinoma in cirrhotic patients with indeterminate liver nodules[J]. European Radiology, 2020, 30(1):558–570.

Figures

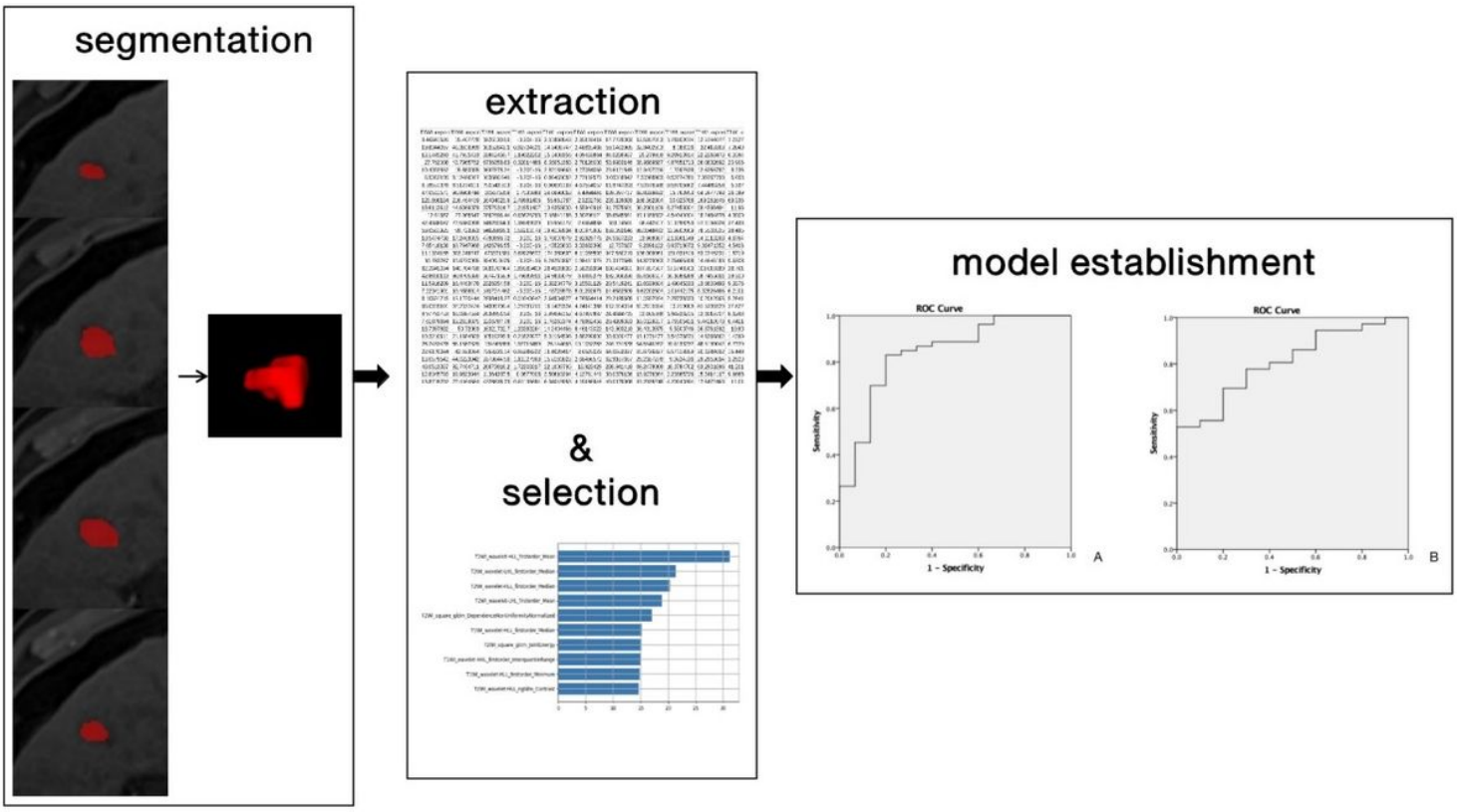

Figure 1

Flow chart of radiomics model establishment

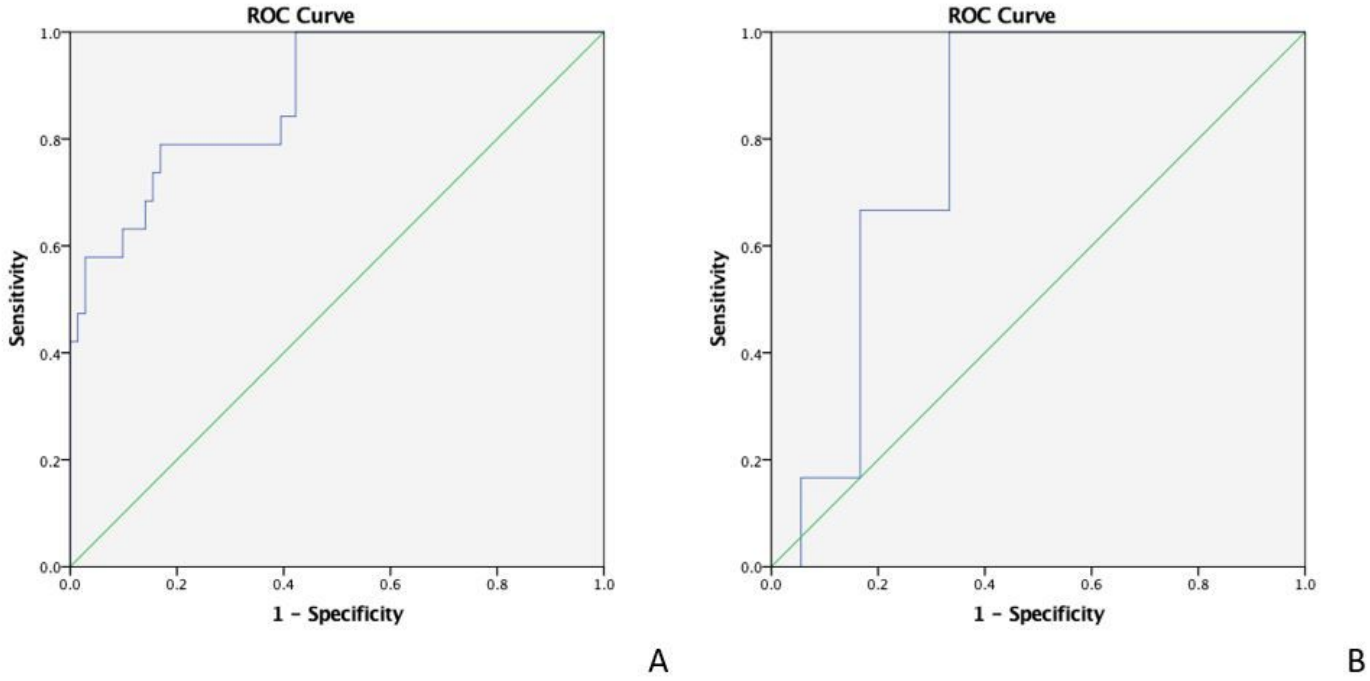

Figure 2

ROCs of radiomics model based on T1WI (A: ROC of training group; B: ROC of test group)

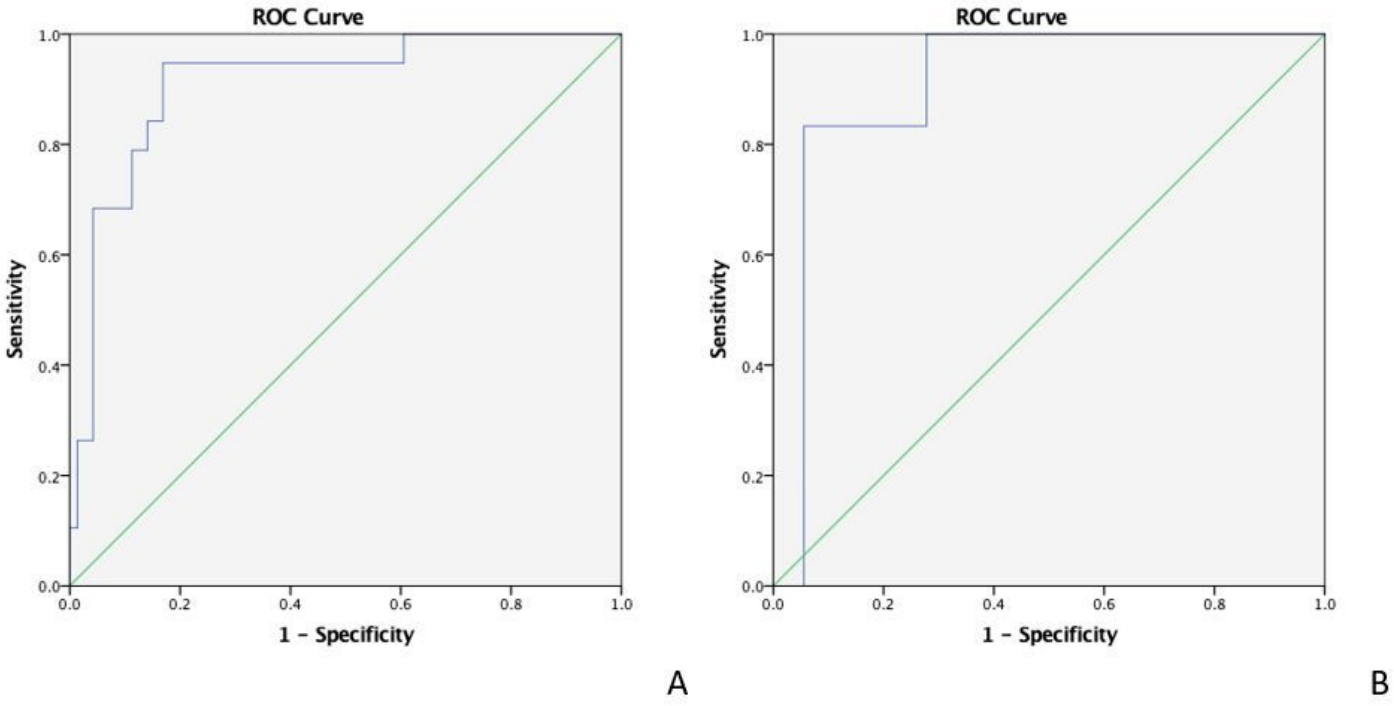

Figure 3

ROCs of radiomics model based on T2WI (A: ROC of training group; B: ROC of test group)

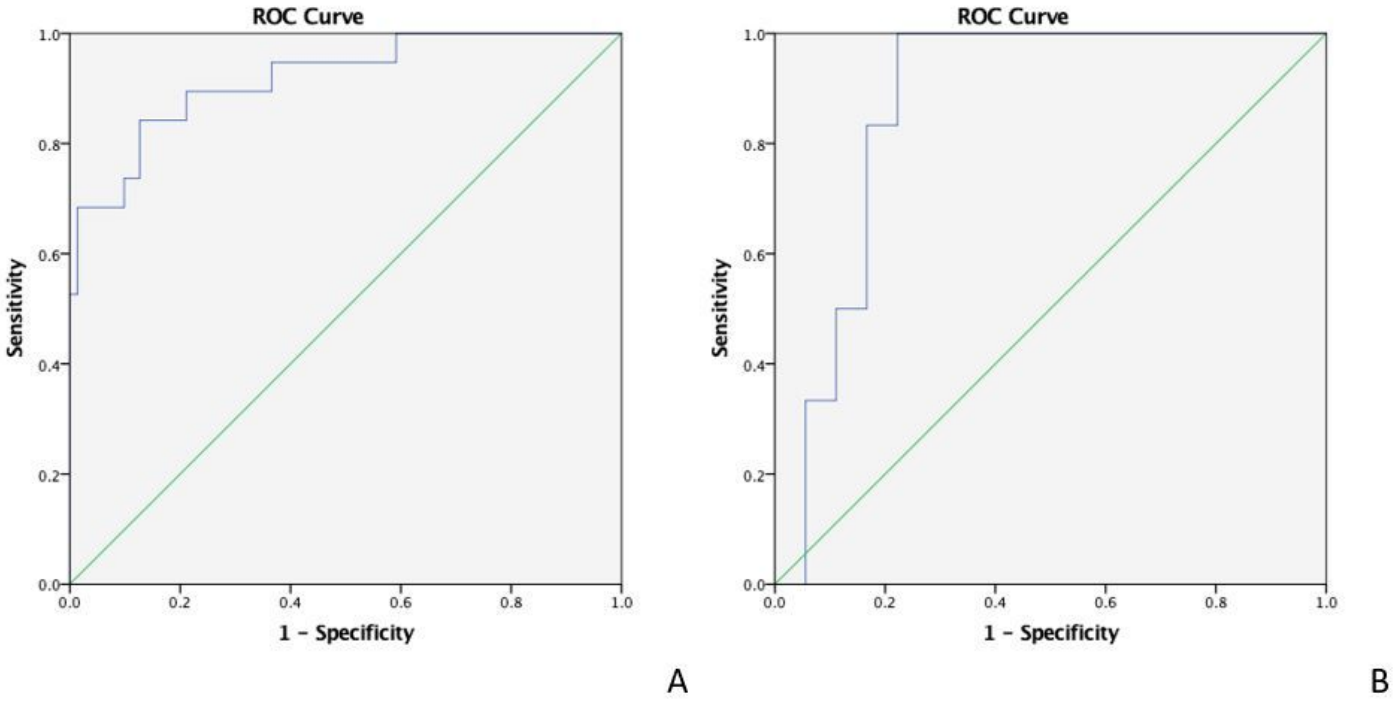

Figure 4

ROCs of radiomics model based on T1WI+FS-T2WI (A: ROC of training group; B: ROC of test group)

Supplementary Files

This is a list of supplementary files associated with this preprint. Click to download.

- SupplementaryInformation.docx